ELSEVIER

Journal of Molecular Catalysis A: Chemical 95 (1995) 211–222

JOURNAL OF MOLECULAR CATALYSIS A: CHEMICAL

CO oxidation over $Pd/FeSbO_4$ catalyst

M.M. Gadgil, S.K. Kulshreshtha *

Chemistry Division, Bhabha Atomic Research Centre, Bombay-400 085, India

Received 5 November 1993; revised 15 July 1994; accepted 7 October 1994

Abstract

Based on ^{57}Fe Mössbauer effect and powder X-ray diffraction measurements it is shown that amorphous $FeSbO_4$ prepared by coprecipitation method, transforms to crystalline form at $\simeq 1125$ K and during hydrogen reduction it decomposes to individual oxides like Fe_3O_4 and Sb_2O_3. On palladium impregnation, the reduction rate of $FeSbO_4$ is enhanced due to spillover of activated hydrogen from Pd centres to support oxide. From the comparative study of the catalytic behaviour of α-Fe_2O_3, α-Sb_2O_4 and $FeSbO_4$ for CO oxidation, it is observed that there are no synergistic effects between Fe^{3+} and Sb^{5+} ions. Pd impregnation facilitates CO oxidation and it occurs through lattice oxygen incorporation. Disproportionation of CO over finer particles of Pd supported over the surface of $FeSbO_4$, has been observed in the temperature region 325–375 K.

Keywords: Antimony; Carbon monoxide; Iron; Mössbauer effect; Oxidation; XRD

1. Introduction

Iron antimonate, $FeSbO_4$, has been found to be an active and selective catalyst for allylic oxidation and ammoxidation of olefins and its physicochemical characteristics have been investigated by many authors [1–6]. The Sb/Fe ratio used for the preparation of catalyst, has profound effect on the activity and selectivity for the product formation. Whereas the excess antimony oxide, if present along with $FeSbO_4$ is selective for partial oxidation, the presence of α-Fe_2O_3 phase leads to complete oxidation and thus loses its selectivity. Various suggestions [7–15] have been given to explain this increase in selectivity of $FeSbO_4$ catalyst having excess antimony oxide. The most accepted explanation is the surface alteration of the catalyst sample due to higher volatility of excess antimony oxide. Catalytic properties of this system are found to depend on the method of preparation. The coprecipitation method gives the most homogeneous mixture and allows $FeSbO_4$ formation at relatively lower temperatures. However, even for stoichiometric ratio of Sb/Fe = 1.0, the formation of α-Fe_2O_3 along with $FeSbO_4$ has been reported [15,17–20] and the reasons for its formation are not well understood. The two most probable explanations proposed for the formation of α-Fe_2O_3 are the selective evaporation of antimony oxide during calcination process and the formation of an antimony rich rutile phase having general formula $(Fe_{1-x}Sb_x)SbO_4$. The Sb/Fe ratio greater than one, has been found to be responsible for the formation of small amount of Fe^{2+} specie [6,13–16] which is proposed to be the active phase for the selective oxidation of olefins. Sala and Trifiro [8] proposed $Fe_2Sb_2O_7$ or $FeSb_2O_6$ as the selective phase. The reasons for

* Corresponding author.

SSDI 1381-1169(94)00027-1

the formation of ferrous species as well as the nature of the compound it forms with antimony oxide, is not well understood. The role played by individual cations of $FeSbO_4$, during catalytic oxidation of olefins is also not well understood. According to Straguzzi et al. [12] Fe^{3+} ion gives its bonded oxygen to the olefin and gets reduced which is reoxidised by the neighbouring Sb^{5+} ion. The reduced antimony ions take up oxygen from reactants and thus functions as an oxygen carrier.

In the present communication we report the calcination and hydrogen reduction behaviour of $FeSbO_4$ with and without Pd metal impregnation to see the role of spillover of activated gases from metal centres to support oxide and the reduction pathway of $FeSbO_4$. The CO oxidation activity of these catalyst samples and the constituent oxides (α-Fe_2O_3 and α-Sb_2O_4) are also reported to show that no synergistic effects have been observed for the mixed oxide system. The influence of noble metal impregnation on the CO oxidation activity of $FeSbO_4$ is also reported.

2. Experimental

The mixed hydroxide of iron and antimony was prepared by reverse coprecipitation method from the respective chloride solutions of Fe(III) and Sb(V) taken in equimolar ratio using ammonium hydroxide. The coprecipitate was filtered, washed thoroughly with water and dried in oven at 395 K for 12 h. The chemical analysis of the bulk samples was carried out to determine Fe contents. The oven dried sample was used for calcination study. Small portions of this sample were calcined at various temperatures from 775 K to 1375 K for 8 h duration. The product formation and the changes in crystallinity were monitored by X-ray diffraction (XRD) and ^{57}Fe Mössbauer techniques. Powder X-ray diffraction patterns were recorded using monochromatised Cu-K_α radiation. The source used for Mössbauer study was ^{57}Co in Rh matrix and all isomeric shift values (δ) are reported with respective to α-Fe metal. The relative composition of few representative samples was determined by EDAX using 25 keV electron to generate characteristic X-rays.

The hydroxides of iron and antimony were prepared separately by precipitation from their respective chloride solutions and drying in an oven at 395 K for 12 h. The hydroxides were calcined in air at 775 K for 4 h and were found to be pure α-Fe_2O_3 and α-Sb_2O_4 from XRD analysis.

The crystalline $FeSbO_4$ sample used for reduction study was obtained by heating the coprecipitate at 1125 K for 8 h and showed well defined XRD pattern characteristic of rutile phase. Palladium impregnated crystalline $FeSbO_4$ was prepared from this 1125 K heated $FeSbO_4$ sample using $PdCl_2$ solution so as to get $\simeq 2\%$ impregnation of Pd by weight. Here after this sample is referred as sample B. This impregnated palladium chloride was reduced to metallic form by heating the sample in hydrogen flow at 450 K for 2 h which is well below the reduction temperature of $FeSbO_4$. The reduction behaviour of these crystalline $FeSbO_4$ and $Pd/FeSbO_4$ samples was studied by placing them separately in two compartments of a quartz boat and simultaneously heating them in the temperature range 575 K to 875 K for 2 h each in flowing hydrogen. Every time a fresh sample of $FeSbO_4$ and $Pd/FeSbO_4$ was taken for reduction at a particular temperature. After heating, the samples were cooled to room temperature in hydrogen flow and taken out for characterisation.

CO oxidation reaction was carried out on crystalline samples of $FeSbO_4$, $Pd/FeSbO_4$, α-Fe_2O_3 and α-Sb_2O_4 catalysts by placing $\simeq 0.5$ g of a catalyst in a tubular stainless steel reactor of i.d. 0.4 cm, using pulse method. Two samples of $Pd/FeSbO_4$ catalysts, used for this study, were prepared by two different methods. In the first method, the catalyst was prepared by impregnating palladium chloride on the coprecipitated amorphous mixed hydroxide of iron and antimony and subsequently heating it at 1125 K for 8 h in air which gives palladium oxide impregnated on crystalline $FeSbO_4$, here after referred as sample A. This sample and the sample B were independently loaded in the catalytic reactor and heated

in-situ in flowing hydrogen at 450 K for 2 h and cooled to room temperature in flowing hydrogen to generate palladium metal before carrying out the CO oxidation study. These two methods were adopted to investigate the effect of sintering of impregnated palladium metal on its CO oxidation behaviour.

One of the following three pretreatments, was given to all the catalysts before carrying out CO oxidation experiment. (i) Heating in helium at 625 K for 2 h, to remove moisture, and cooled in helium to room temperature, (ii) heating in oxygen at 625 K for 2 h followed by heating in helium at 625 K for 2 h, to oxidise the catalyst support and to remove adsorbed oxygen, and cooled in helium to room temperature, and (iii) heating in hydrogen at 525 K for 2 h to create the reduced surface of the support material, followed by heating in helium at 625 K for 2 h, to remove adsorbed hydrogen, and cooled in helium to room temperature. After this pretreatment, 100 mm^3 pulses of either $(CO+O_2)$ (1:1) mixture or only CO were injected over the catalyst surface under helium flow of $\simeq 30$ cm^3/min at variable temperatures and the effluent gases were analysed by gas chromatographic method using Porapak Q column and thermal conductivity detector.

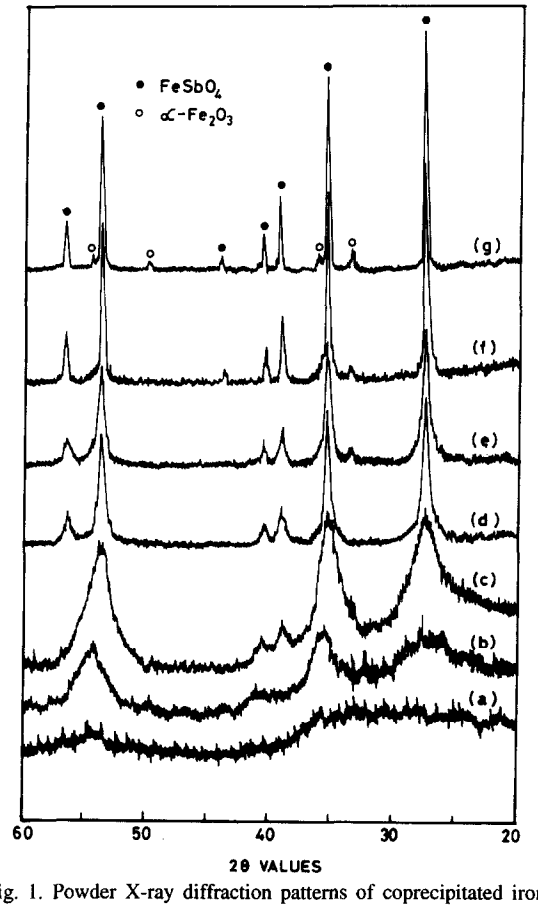

Fig. 1. Powder X-ray diffraction patterns of coprecipitated iron–antimony mixed hydroxide calcined for 8 h at (a) 400 K (oven dried), (b) 775 K, (c) 1025 K, (d) 1075 K, (e) 1125 K, (f) 1175 K and (g) 1375 K.

3. Results and discussion

3.1. Calcination behaviour

Fig. 1 shows the XRD patterns of coprecipitated mixed hydroxide sample calcined at different temperatures in air. The oven dried sample does not show any diffraction pattern suggesting the amorphous nature of the coprecipitated oxide. The sample heated at $\simeq 775$ K for 8 h shows very broad lines characteristic of rutile structure indicating the formation of fine crystallites of $FeSbO_4$ in the mixed oxide. Heating at still higher temperatures leads to the improved crystallinity as can be seen from the reduced width of the XRD peaks observed for the sample heated at 1125 K for 8 h. It may be mentioned that in addition to the formation of crystalline $FeSbO_4$, Bragg reflections characteristic of α-Fe_2O_3 having very small intensity are also noticed for the samples heated at 1125 K and higher. To understand the origin of this α-Fe_2O_3, a portion of $FeSbO_4$ sample already calcined at 1375 K, was further calcined at the same temperature for another 24 h duration. The sample does not show any increase in the intensity of α-Fe_2O_3 peaks. This suggests that α-Fe_2O_3 is partially left out due to the selective evaporation of antimony oxide during calcination before its complete reaction with α-Fe_2O_3 to form $FeSbO_4$ and not because of its selective evaporation from the $FeSbO_4$ matrix as seen from the chemical analysis and X-ray fluorescence yield of $FeSbO_4$ samples calcined at different temperatures. The bulk Fe analysis of the samples calcined at 400, 575, 775,

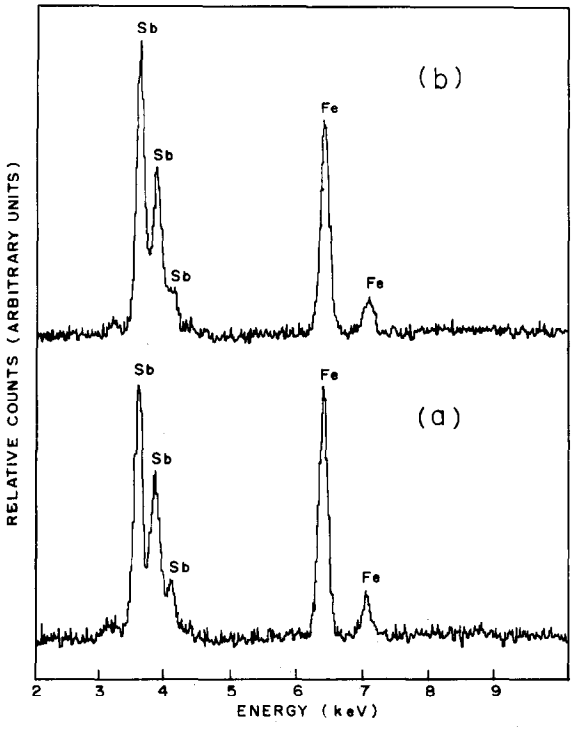

Fig. 2. EDAX patterns of $FeSb_2O_4$ samples calcined for 8 h at (a) 775 K and (b) 1375 K recorded with 25 keV electrons used to generate characteristic X-rays.

1125 and 1375 K for a fixed duration of 8 h, was found to be 24.8, 25.3, 27.5, 27.6 and 27.3%, respectively. These values are slightly more than the theoretical value of iron contents for the stoichiometric $FeSbO_4$ (23.1%). These results suggest that at lower temperatures of calcination there is some loss of Sb before the formation of $FeSbO_4$ at 775 K. Calcination at temperatures above 775 K did not change the iron concentration suggesting that there is no more loss of antimony oxide after the formation of $FeSbO_4$ compound. Fig. 2(a and b) shows the EDAX results for two representative samples of $FeSbO_4$ which have been prepared by calcining the oven dried coprecipitate at 775 and 1375 K for 8 h, respectively. From this figure it is clear that Sb/Fe ratio on the surface has significantly increased for the sample calcined at 1375 K. Further unlike chemical analysis, the EDAX analysis carried out using 25 keV electrons whose penetration is confined up to a depth of $\simeq 1.8$ microns, showed that the Sb/Fe ratio for the samples calcined at 775 K and 1375 K is 1.03 and 1.09, respectively, which is originating because of the selective evaporation of antimony oxide from the bulk. Based on these observations it is possible to rule out the suggestions of Centi and Trifiro [19] about the formation of α-Fe_2O_3. These authors have ruled out the possibility of selective evaporation of antimony oxide during calcination process and have suggested the formation of rutile phase with excess antimony namely $(Fe_{1-x}Sb_x)SbO_4$ thereby leading to the formation of α-Fe_2O_3. However, under such situation the Sb/Fe ratio is expected to change neither in the bulk nor on the surface during calcination process. This is unlike what has been observed in the present study using both chemical analysis and EDAX measurements. Further, no change in the unit cell volume has been observed for $FeSbO_4$ samples calcined at different temperatures ($1075 \leq T/K \leq 1375$) which is well above the temperature of rutile phase formation, suggesting that there is no change in the composition of $FeSbO_4$ lattice above 975 K and selective evaporation of antimony oxide from $FeSbO_4$ matrix does not occur. The observed value of the unit cell volume in the present study is 66.0 $Å^3$ is in good agreement with the value reported by Centi et al. [19] for their stoichiometric composition of $FeSbO_4$ calcined at 1175 K and above. The observed Sb enrichment on the surface is quite similar to what has been reported earlier from the XPS studies of $Sb_2O_4 + SnO_2$ system [21], where it was suggested that during calcination at 875 K, due to selective evaporation of Sb from the bulk, the surface gets enriched with antimony up to a depth of $\simeq 50$ Å. It may be mentioned that the crystallisation of α-Fe_2O_3 is significantly retarded due to its coprecipitation with antimony oxide as seen from the XRD pattern of the sample heated at 775 K for 8 h and shown in Fig. 1(b), because the oven dried sample of iron oxide alone, when heated at $\simeq 775$ K for 8 h, was found to be well crystalline.

The ^{57}Fe Mössbauer spectra recorded at room temperature for the coprecipitated mixed hydroxide samples calcined at different temperatures are

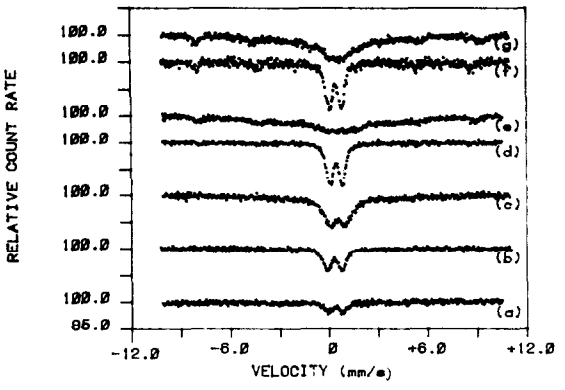

Fig. 3. ^{57}Fe Mössbauer spectra recorded at room temperature for coprecipitated iron–antimony mixed hydroxide calcined for 8 h at (a) 400 K (oven dried), (b) 775 K, (d) 1125 K, and (f) 1375 K. The spectra recorded at 78 K for the samples calcined at (c) 775 K, (e) 1125 K and (g) 1375 K.

shown in Fig. 3. All spectra show quadrupole doublet. The values of various Mössbauer parameters obtained from the fitting of these spectra show that on increasing calcination temperature, the line width and quadrupole splitting values (ΔE_q) are decreased. The Mössbauer spectra of the samples calcined at 1125 K and above, for which the XRD patterns show good crystallinity, show a well defined quadrupole doublet with $\delta = 0.37$ mm/s and $\Delta E_q = 0.75$ mm/s indicating the existence of high spin Fe^{3+} in a distorted octahedral environment. These values are in very good agreement with those reported earlier [22] for $FeSbO_4$. This indicates that the reaction between iron oxide and antimony oxide is complete by 1125 K. The spectrum of the sample calcined at 1375 K (Fig. 3(f)) shows the presence of a magnetic sextet corresponding to α-Fe_2O_3 in addition to a quadrupole doublet of $FeSbO_4$, which is consistent with XRD results. For lower temperatures of calcination the unreacted α-Fe_2O_3 if present, is in the form of very fine particles dispersed in an amorphous matrix. These fine particles of α-Fe_2O_3, due to superparamagnetic effects, give rise to a quadrupole doublet which is superimposed over the quadrupole doublet of $FeSbO_4$ formed due to partial completion of reaction. The ^{57}Fe Mössbauer spectra of the samples calcined at 775, 1125 and 1375 K, when recorded at 78 K, clearly showed the broadening of the central doublet and the appearance of a magnetic sextet (viz. Fig. 3(e and g)) which is the characteristic feature of superparamagnetic particles. No detectable difference in the calcination behaviour of $FeSbO_4$ and Pd/$FeSbO_4$ is observed.

3.2. Reduction behaviour

A representative set of XRD patterns, depicting the reduction behaviour of crystalline $FeSbO_4$ at different temperatures, is shown in Fig. 4. Since the reduction study at variable temperatures is carried out by taking every time a fresh sample of $FeSbO_4$, the relative amounts of various products as revealed by XRD patterns, are not varying quantitatively in relation with the reduction temperature. From Fig. 4(a) and (b) it is clear that although there is no bulk reduction of crystalline

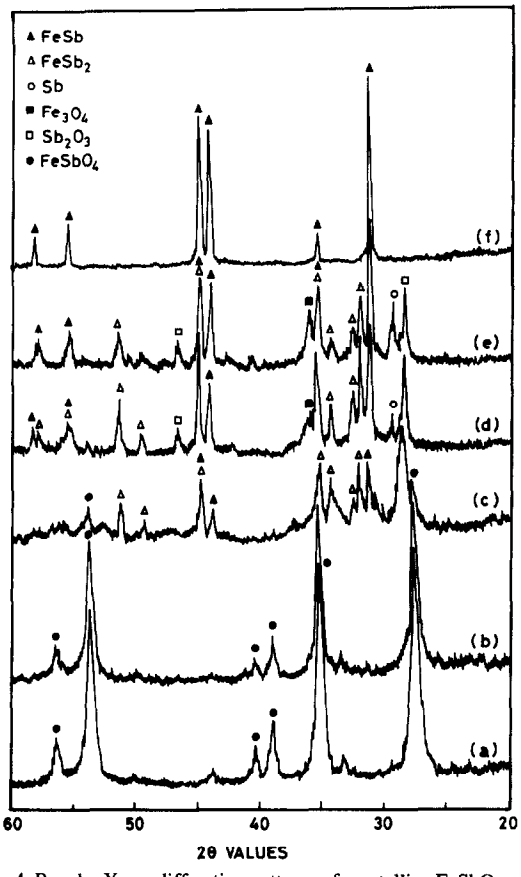

Fig. 4. Powder X-ray diffraction patterns of crystalline $FeSbO_4$ samples heated in hydrogen flow for 2 h at (a) 575 K, (b) 625 K, (c) 650 K, (d) 675 K, (e) 775 K and (f) 825 K.

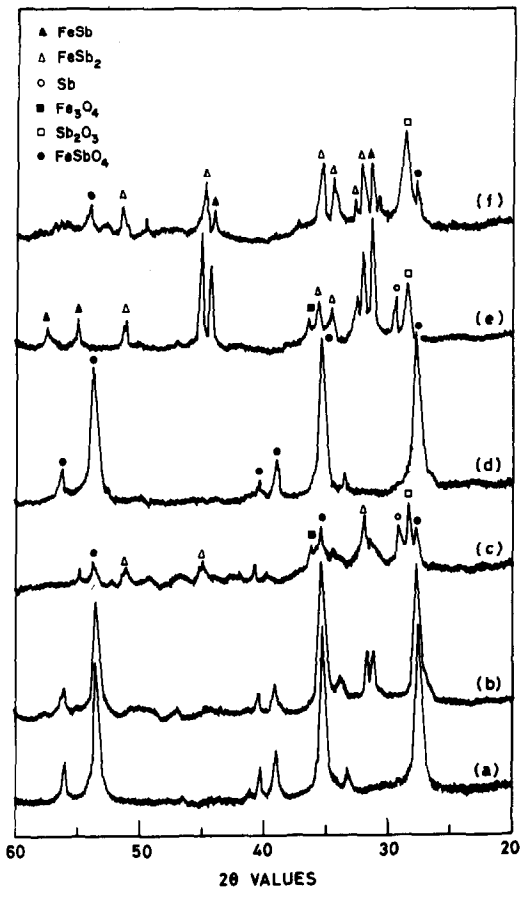

Fig. 5. Powder X-ray diffraction patterns of $Pd/FeSbO_4$ samples heated in hydrogen flow for 2 h at (a) 575 K, (b) 600 K, (c) 625 K and (e) 650 K. X-ray diffraction patterns of $FeSbO_4$ samples heated in hydrogen flow for 2 h at (d) 625 K and (f) 650 K are given for comparison.

$FeSbO_4$ up to a reduction temperature of 625 K, the possibility of surface reduction can not be ruled out. Fig. 4(c) shows the formation of Sb_2O_3, $FeSb_2$ and FeSb along with minor amount of unreduced $FeSbO_4$. The $FeSbO_4$ samples reduced at higher temperatures (at 675 K and 775 K, Fig. 4(d) and 4(e)) show the formation of Sb_2O_3, Fe_3O_4, Sb metal and intermetallics $FeSb_2$ and FeSb in varying amounts. Further, at reduction temperature of 825 K the main product of reduction, FeSb, is obtained (Fig. 4(f)). It may be specifically mentioned that the crystalline $FeSbO_4$ used for the present reduction study contained detectable amount of α-Fe_2O_3 which may be expected to give the corresponding amount of Fe metal on reduction. However, the formation of Fe metal is not clearly seen in the XRD pattern shown in Fig. 4(f) because of the two possible reasons. (i) The prominent (110) Bragg reflection of bcc Fe placed at $2\theta = 44.7°$ is completely masked by the intense (110) Bragg reflection of FeSb placed at $2\theta = 44.3°$ due to its very small abundance. The other less intense reflection of α-Fe lie at $2\theta > 60°$ and are not seen in this figure. (ii) The other most probable reason is the nonstoichiometric nature of FeSb phase which is known to exist as a hexagonal single phase with significantly excess concentration of Fe with an atomic ratio of $1.08 \leq Fe/Sb \leq 1.38$ [23–25]. Further, it has also been reported that the values of cell parameters and their ratio c/a depends on the Fe/Sb ratio. The observed values of $a = 4.098$ Å and $c = 5.145$ Å in the present study are corresponding to the Fe rich compositions [23]. The formation of Sb_2O_3, at initial stages of reduction (at 650 K) as a major product, indicates that the reduction of $FeSbO_4$ occurs by decomposition to give its individual oxides of lower oxidation state, as shown below.

$$6FeSbO_4 \xrightarrow{H_2} 2Fe_3O_4 + 3Sb_2O_3$$

Although, at 650 K temperature of reduction, the formation of Fe_3O_4 is not clearly seen in XRD pattern possibly due to its amorphous and finely dispersed form, it can be clearly observed at high temperature of reduction. As the reduction of Sb_2O_3 to Sb metal is faster than that of Fe_3O_4 to Fe metal, the Sb metal forms in excess of Fe metal and gives rise to $FeSb_2$. On complete reduction of these different oxide phases, the expected single product FeSb, is formed. The Fe^{2+} compounds with antimony oxide, e.g. $FeSb_2O_6$, $Fe_2Sb_2O_7$ and $FeSb_2O_4$ which are said to be active and selective phases in olefin oxidation, are not formed as bulk material during hydrogen reduction of $FeSbO_4$ possibly because of the difference in reducing power of hydrogen and olefins. The results obtained from the XRD patterns of reduced samples of $FeSbO_4$ and $Pd/FeSbO_4$ have revealed that although the reduction of $FeSbO_4$ is facilitated by Pd impregnation, the reduction pathway is the same for both the samples. For $Pd/FeSbO_4$ the

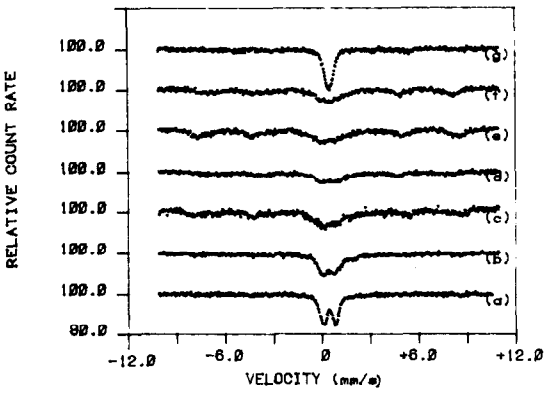

Fig. 6. ^{57}Fe Mössbauer spectra recorded at room temperature for $FeSbO_4$ samples heated in hydrogen flow for 2 h at (a) 625 K, (b) 650 K, (d) 675 K, (f) 775 K and (g) 825 K. The spectra recorded at 78 K for the samples heated in hydrogen flow at (c) 650 K and (e) 675 K.

reduction is initiated at $\simeq$600 K (Fig. 5(b)) which is lower than that observed for $FeSbO_4$ (650 K) as can be seen from Fig. 5. This is due to activation and spillover of hydrogen from palladium metal sites to $FeSbO_4$ support causing its reduction at relatively lower temperature.

The representative ^{57}Fe Mössbauer spectra recorded at room temperature for the reduced samples of $FeSbO_4$ are shown in Fig. 6. The results are complementary to the XRD results. Fig. 6(a) shows quadrupole doublet having $\delta = 0.35$ mm/s and $\Delta E_q = 0.75$ mm/s indicating no bulk reduction of $FeSbO_4$ at 625 K. The broad unresolved two sextets expected for the fine particles of Fe_3O_4 are seen in Fig. 6(f) along with the spectra of $FeSb_2$ and FeSb products. Because of very complex nature it is not possible to fit this spectrum to evaluate the relative contribution of different phases. The formation of Fe_3O_4 at lower temperature of reduction (in Fig. 6(b and d)) is not clearly seen due to the finely dispersed nature of these small particles which do not exhibit magnetic pattern. The presence of Fe_3O_4 is better demonstrated from the liquid nitrogen temperature Mössbauer spectra of the samples reduced at 650 and 675 K, which are shown in Fig. 6(c) and (e), respectively. Presence of $FeSb_2$ is revealed by paramagnetic quadrupole doublet having $\delta \simeq 0.47$ mm/s and $\Delta E_q \simeq 1.28$ mm/s whereas FeSb exhibits an unresolved quadrupole doublet having $\delta = 0.41$ mm/s and $\Delta E_q = 0.285$ mm/s. These parameters are in agreement with those reported for $FeSb_2$ and FeSb in literature [26]. At the end of reduction of $FeSbO_4$ the expected product, FeSb, is formed which is shown in Fig. 6(g). The existence of free Fe metal is not seen in this figure because the FeSb formed is nonstoichiometric with atomic ratio of Fe/Sb > 1.0.

3.3. CO oxidation reaction

Fig. 7 shows the plots of yield of CO_2 as a function of temperature when 100 mm^3 pulse of either CO or $(CO + O_2)$ mixture is injected over the surface of crystalline $FeSbO_4$ catalyst pretreated in helium at 625 K for 2 h. It can be observed that when a pulse of $(CO + O_2)$ is injected over the surface of catalyst, CO oxidation initiates at $\simeq$475 K and is almost complete by $\simeq$575 K (viz. Fig. 7(b)). Unlike this, when only

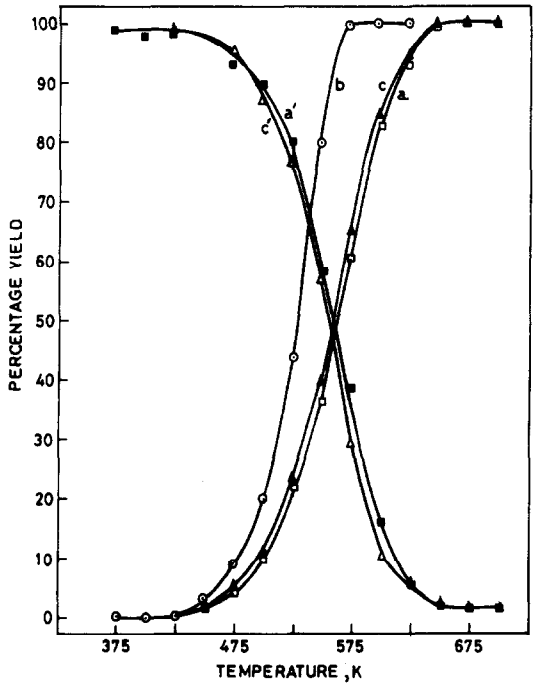

Fig. 7. Percentage yield of CO_2 over the surface of crystalline $FeSbO_4$, heated in helium at 625 K for 2 h when (a) CO pulses were injected (□), (b) $(CO + O_2)$ pulses were injected (○) and (c) CO pulses were injected over the surface of $FeSbO_4$ pretreated with oxygen (625 K, 2 h) followed by heating in helium at 625 K for 2 h (▲). The yield of unreacted CO corresponding to Fig. (a) and (c) are shown in Fig. (a') (■) and (c') (△).

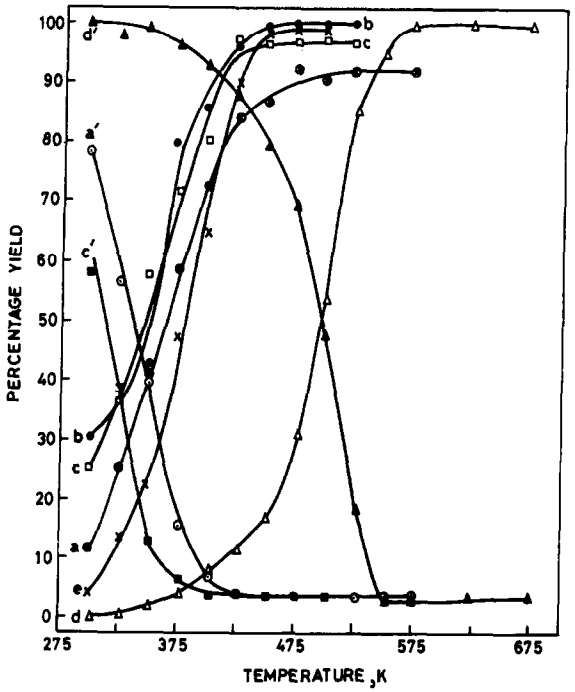

Fig. 8. Percentage yield of CO_2 when either CO or $(CO + O_2)$ pulses were injected over the surface of $Pd/FeSbO_4$ (sample A) after giving following treatments in sequence (a) helium at 625 K for 2 h and CO pulses (⊗), (b) helium at 625 K for 2 h and $(CO + O_2)$ pulses (●), (c) oxygen at 625 K for 2 h followed by heating in helium at 625 K for 2 h and CO pulses (□), (d) hydrogen at 525 K for 2 h followed by heating in helium at 625 K for 2 h and CO pulses (△) and (e) hydrogen at 525 K for 2 h followed by heating in helium at 625 K for 2 h and $(CO + O_2)$ pulses (×). The yield of unreacted CO corresponding to Fig. (a), (c) and (d) are shown in Fig. (a') (○), (c') (■) and (d) (▲).

CO pulse has been injected, the CO oxidation although complete, but occurs at relatively higher temperature (Fig. 7(a)). Further, the yield of CO_2 for $FeSbO_4$ sample pretreated at 525 K, in H_2 was found to be much lower when only CO pulses were injected. These results possibly suggest that CO oxidation occurs through lattice oxygen abstraction and oxygen present in the feed gas mixture facilitates it by surface rejuvenation. The role of lattice oxygen during CO oxidation over the surface of oxide systems has been investigated by a number of investigators [27,28] using ^{18}O enriched reactants and it has been shown that oxygen from the surface layers is used for CO oxidation and the high mobility of lattice oxygen to surface sites facilitates this oxidation. Keulks [27] has studied the CO oxidation over the surface of bismuth molybdate catalyst and emphasised the role of oxygen diffused from the subsurface layers to the surface sites available on the catalyst. Conner et al. [28] have studied the oxidation of CO over NiO catalyst and suggested that there are two reaction mechanisms for CO oxidation to form CO_2, and surface oxygen is mainly reacting with CO. The oxygen pretreatment given to the catalyst at 650 K for 2 h has not shown any improvement in the catalytic activity of $FeSbO_4$ (Fig. 7(c)) as compared to its activity before oxygen pretreatment (Fig. 7(a)) indicating that no adsorbed oxygen is left over the surface of $FeSbO_4$ after pretreatment in oxygen (625 K, 2 h) followed by heating in flowing helium at 625 K for 2 h. Fig. 7(a') and (c') show the amount of unreacted CO eluted during the CO_2 oxidation experiments corresponding to the results of CO yield, shown in Fig. 7(a) and (c), respectively. These results indicate that the unreacted CO does

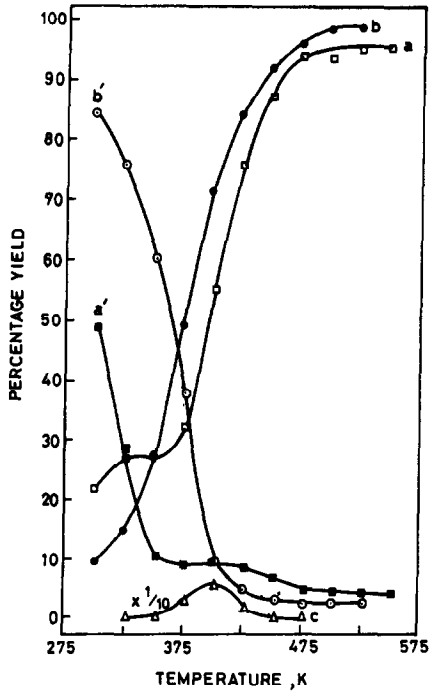

Fig. 9. Percentage yield of CO_2 when only CO pulses were injected over the surface of (a) $Pd/FeSbO_4$ (sample B) (□) and (b) $Pd/FeSbO_4$ (sample A) (●) after the same pretreatments and their corresponding unreacted CO eluted are shown in Fig. (a') (■) and (b') (○). The yield of CO_2 on injection of oxygen pulse over sample B after elution of CO_2 and unreacted CO, is shown in Fig. (c) (△).

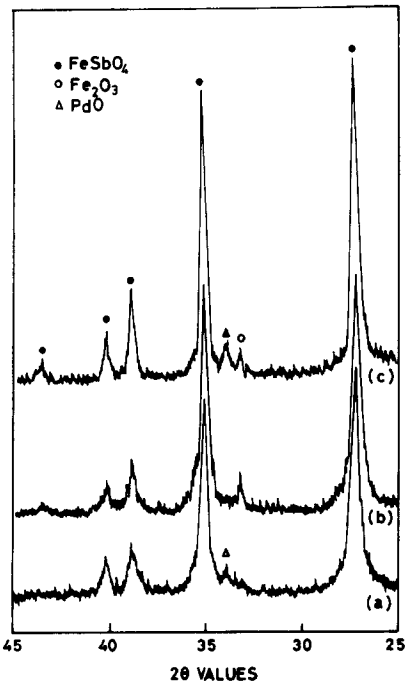

Fig. 10. Powder X-ray diffraction pattern of (a) catalyst sample A (coprecipitate, impregnated by $PdCl_2$ and calcined at 1125 K for 8 h) and (b) catalyst sample B (coprecipitate, calcined at 1125 K for 8 h, impregnated by $PdCl_2$ and heated at 675 K for 4 h). (c) coprecipitate, impregnated by $PdCl_2$ and calcined at 1175 K for 8 h.

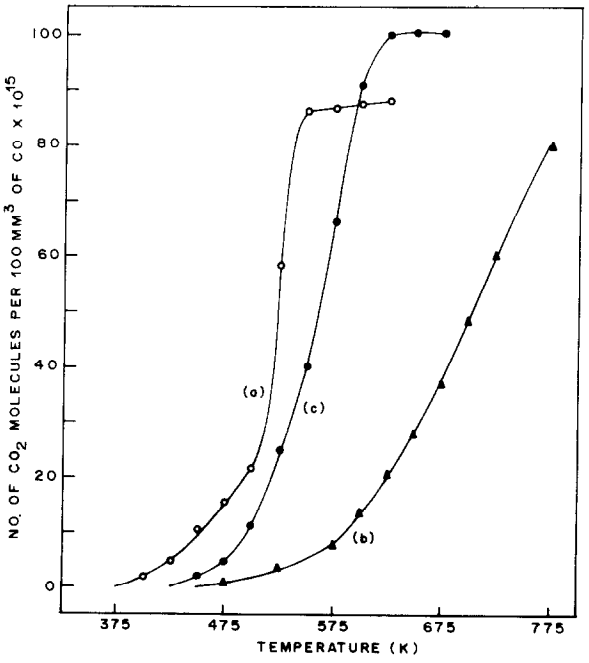

Fig. 11. Yield of CO_2 molecules per unit surface area of the catalyst for every 100 mm^3 pulse of CO injected over (a) α-Fe_2O_3 with surface 22.62 m^2/g (○), (b) α-Sb_2O_4 with surface area 14.28 m^2/g (▲) and (c) crystalline $FeSbO_4$ with surface area 19.55 m^2/g (●).

not remain adsorbed over the surface of $FeSbO_4$ catalyst at the reaction temperatures ($300 \leq T/K \leq 675$).

Fig. 8(a) depicts the plot of CO_2 yield as a function of temperature for $Pd/FeSbO_4$ (sample A) catalyst pretreated in helium, when only CO pulses are injected. On comparison of this plot with Fig. 8(b) where pulses of $(CO+O_2)$ mixture are injected over similarly pretreated catalyst, reveals that oxygen present in the reactant gas mixture facilitates CO oxidation. The oxygen pretreatment of $Pd/FeSbO_4$ catalyst at 625 K for 2 h has enhanced the catalytic activity for CO oxidation as shown in Fig. 8(c) where only CO pulses are injected. This indicates that the PdO_x species which may be formed due to oxygen pretreatment, are reactive towards CO oxidation and facilitates the reaction. The amount of unreacted CO eluted

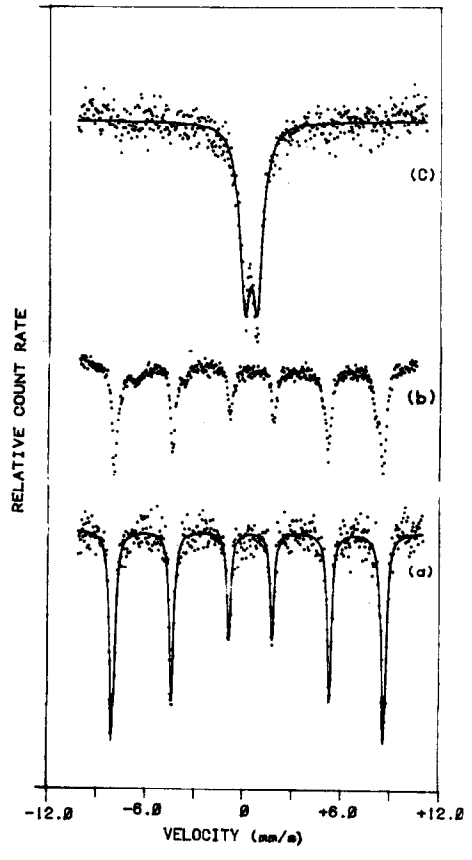

Fig. 12. ^{57}Fe Mössbauer spectra of the mixture of (a) (α-$Fe_2O_3 + Sb_2O_4$), (b) after heating in CO flow at 625 K for 2 h exhibiting the partial reduction of α-Fe_2O_3 and (c) $FeSbO_4$ after heating in CO flow at 625 K for 2 h.

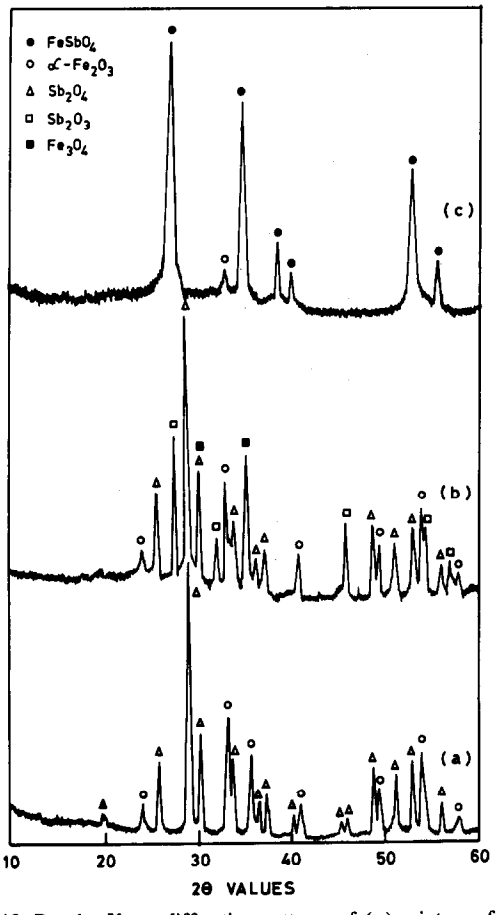

Fig. 13. Powder X-ray diffraction patterns of (a) mixture of (α-$Fe_2O_3 + Sb_2O_4$), (b) mixture of (α-$Fe_2O_3 + Sb_2O_4$) heated in CO flow for 2 h at 625 K and (c) $FeSbO_4$ after heating in CO flow at 625 K for 2 h.

at different temperatures which are shown in Fig. 8(a′) and (c′) correspond to the yields of CO_2 depicted in Fig. 8(a) and (c). An analysis of the results shown in Fig. 8(a) and (a′) suggests that the total yield of CO_2 can not be understood in terms of the CO disproportionation alone and lattice oxygen from support oxide is being used as the Pd sites are not oxidised under the experimental conditions. On comparison of CO oxidation activity of $Pd/FeSbO_4$ and $FeSbO_4$ when only CO pulses are injected after the same pretreatment (viz. Fig. 8(a) and 7(a)), it is observed that the CO oxidation activity is significantly improved due to Pd metal impregnation over the surface of $FeSbO_4$. Based on these results it can be inferred that activation of CO on palladium sites and its spillover to the support takes place which enhances the CO oxidation activity due to lattice oxygen incorporation. Further a comparison of the results shown in Fig. 8(a and a′) and 8(c and c′) suggests that the oxygen treatment given to the catalyst has enhanced the yield of CO_2. This may possibly be arising due to the availability of additional oxygen from PdO_x type of species produced during oxygen pretreatment given to the catalyst. The hydrogen pretreatment of $Pd/FeSbO_4$ catalyst at 525 K for 2 h has significantly lowered the CO oxidation activity (Fig. 8(d)). This is due to surface reduction of $FeSbO_4$ and thereby affecting the availability of lattice oxygen. When pulses of ($CO + O_2$) mixture are injected over this reduced surface the activity of $Pd/FeSbO_4$ increased drastically (Fig. 8(e)) as a result of rejuvenation of the surface lattice oxygen of the catalyst with the help of oxygen present in reactant gas mixture.

The $Pd/FeSbO_4$ catalyst prepared by another method, i.e. sample B, has behaved differently in CO oxidation experiments as compared to sample A as can be seen from the results presented in Fig. 9(a) and (b) for the same pretreatment. The yield of CO_2, when only CO pulses are injected over sample B, shows a clear discontinuity in the region 325 K to 375 K in Fig. 9(a) which is absent in Fig. 9(b). This discontinuity in the yield of CO_2 is due to the disproportionation of CO on palladium sites to give active carbon and CO_2. During this process, since two chemisorbed CO molecules are consumed to give only one molecule of CO_2, the yield of CO_2 decreases with increasing temperature and gives rise to this discontinuity. The observed disproportionation step is further confirmed from the formation of CO_2 (Fig. 9(c)) when 80 mm^3 pulse of oxygen is injected over the $Pd/FeSbO_4$ catalyst (sample B) after elution of both CO_2 and unreacted CO, at different temperatures. This CO_2 is formed due to the reaction between oxygen and the active carbon formed over Pd surface during CO disproportionation process. When similar experiments of oxygen injection are carried out over sample A, after CO oxidation and elution of both CO_2 and unreacted CO, the formation of additional CO_2 is not

observed which suggests the absence of CO disproportionation step for this sample. The disproportionation of CO on palladium is reported in literature by many authors [29–32] and it has been shown that the disproportionation takes place only on smaller particles of palladium. For sample A, during calcination process the agglomerates of palladium oxide are formed over the surface of $FeSbO_4$ which on hydrogen reduction lead to the formation of much bigger clusters of Pd metal thereby preventing the CO disproportionation step. Further support to this inference is provided from the appearance of PdO peak in the XRD pattern of sample A ($2\theta = 33.95°$) which is not observed for sample B calcined at 675 K for 4 h as can be seen from the XRD patterns shown in Fig. 10(a) and (b). This observation is in conformity with the results reported earlier [29–32] that CO disproportionation occurs only on fine particles of Pd metal.

The CO oxidation activity measured in terms of the number of CO_2 molecules formed per unit surface area when 100 mm^3 pulse of CO were injected over the surface of the crystalline samples of α-Fe_2O_3, α-Sb_2O_4 and $FeSbO_4$, is shown in Fig. 11(a), (b) and (c), respectively. From the comparison of these plots it is observed that α-Fe_2O_3 is the most active for CO oxidation. Unlike this, α-Sb_2O_4 is the least active and complete conversion of CO could not be achieved even up to 775 K. The reducibility character of different oxides can be measured in terms of the change in free energy involved during breaking of the bond between metal and oxygen ions [33]. These values for Fe^{3+}–O and Sb^{5+}–O are 41.67 and 38.60 kcal/mol [34], respectively, which are almost comparable. Similarly, the reduction potential for $Sb^{5+} \rightarrow Sb^{3+}$ (0.70 eV) is quite comparable to the value of $Fe^{3+} \rightarrow Fe^{2+}$ (0.77 eV) [35]. Both these observations suggest that the CO oxidation capability of both the catalysts must be similar which is unlike what has been observed in the present study. The catalytic activity of crystalline $FeSbO_4$ is less than that of α-Fe_2O_3 as seen from Fig. 11(c). Further, no synergistic effects have been observed between Sb^{5+} and Fe^{3+} ions. This is unlike what has been reported by Weng et al. [36] for $MoO_3 + Sb_2O_4$ and $SnO_2 + Sb_2O_4$ systems where significant synergistic effects between Sn–Sb and Mo–Sb ions have been demonstrated. It may further be mentioned that the CO oxidation activity of α-$Fe_2O_3 + SnO_2$ and $Mn_2O_3 + SnO_2$ systems, which do not undergo a chemical reaction to form a new phase, is found to increase significantly as compared to that of the constituents [37]. These observations suggest that the observed activity for $FeSbO_4$ is characteristic of this compound and is significantly better than that observed for α-Sb_2O_4 but less than that of α-Fe_2O_3.

In order to further ascertain the reduction behaviour of Fe^{3+} and Sb^{5+} cations, a mixture of crystalline α-Fe_2O_3 and α-Sb_2O_4 (which were precalcined individually at 775 K) and crystalline $FeSbO_4$ were treated with CO at 625 K for 2 h in continuous flow mode. The ^{57}Fe Mössbauer spectra of the mixed oxide sample clearly showed the formation of Fe_3O_4 due to partial reduction of α-Fe_2O_3 by CO as can be seen from Fig. 12. The X-ray diffraction studies of this CO treated mixed oxide clearly showed the formation of both Fe_3O_4 and Sb_2O_3 as can be seen from Fig. 13(a and b). Unlike this, the X-ray diffraction studies of the crystalline $FeSbO_4$ after treating with CO did not show any bulk transformation of the sample, viz. Fig. 13(c). Similarly, the room temperature ^{57}Fe Mössbauer spectrum of crystalline $FeSbO_4$ treated with CO at 625 K for 2 h did not show the bulk reduction of the sample as can be seen from Fig. 12(c) which is very similar to that observed for the original $FeSbO_4$ sample. However, the low temperature Mössbauer spectra and room temperature magnetisation measurements suggest the formation of Fe_3O_4. These results provide evidence for the surface decomposition of $FeSbO_4$ and reduction of Fe^{3+} species during CO treatment. Further, it is of interest to note that the mechanism of initial reduction of $FeSbO_4$ during hydrogen and CO treatment is almost similar.

4. Conclusions

In conclusion, in the present communication the calcination and hydrogen reduction behaviour of

$FeSbO_4$ catalyst with and without Pd metal impregnation has been investigated and it is observed that the reduction of $FeSbO_4$ takes place by decomposition process and metal impregnation facilitates the reduction at relatively lower temperatures due to spillover of activated hydrogen from Pd centres to the support. The reasons for the formation of α-Fe_2O_3 during calcination of coprecipitated mixed oxides are discussed. The results of CO oxidation presented in this study show that lattice oxygen incorporation is an important mode of CO oxidation for $FeSbO_4$. For Pd impregnated $FeSbO_4$ the CO oxidation occurs at lower temperatures due to spillover of activated CO from metal centres to the support where it reacts with the lattice oxygen. CO disproportionation has been observed for finely dispersed Pd particles at $\simeq$ 325–375 K. This disproportionation is retarded over larger Pd particles formed by agglomeration process during the calcination process of $FeSbO_4$.

Acknowledgements

Authors are extremely grateful to Dr. J.P. Mittal, Director Chemistry Group, for his keen interest and guidance during the course of these investigations. Authors also thank Dr. M.S. Anand for providing the EDAX data. Thanks are due to Kum. R. Sasikala for help in experimental work.

References

[1] C.R. Adams and T. Jennings, J. Catal. 2 (1963) 62.
[2] W.M.H. Sachtler and N.H. de Boer, in Proceedings, 3rd International Congress on Catalysis, Amsterdam, 1964, Vol. 1, p. 252. Wiley, New York, 1965.
[3] M. Petrera, A. Gennaro, N. Burriesci and J.C.J. Bart, Z. Anorg. Allg. Chem. 472 (1981) 179.
[4] F.J. Berry and M.E. Brett, J. Catal. 88 (1984) 232.
[5] R.G. Teller, J.F. Brazdil and R.K. Grasselli, J. Chem. Soc., Faraday Trans. 1, 81 (1985) 1693.
[6] F.J. Berry, J.G. Holden and M.H. Loretto, J. Chem. Soc., Dalton Trans., (1987) 1727.
[7] V. Fattore, Z.A. Fuhrman, G. Manara and B. Notari, J. Catal. 37 (1975) 223.
[8] F. Sala and F. Trifiro, J. Catal. 41 (1976) 1.
[9] F.J. Ulrich, H. Kriegsmann, G. Ohlmann and J. Scheve, in G.C. Bond, P.B. Wells and F.C. Tompkins (Eds.), Proceedings, 6th International Congress on Catalysis, London, 1976, Vol. 2, The Chemical Society, London, 1977, p. 836.
[10] G.I. Straguzzi, K.B. Bischoff, T.A. Koch and G.C.A. Schuit, Appl. Catal. 25 (1986) 257.
[11] M. Carbucicchio, G. Centi and F. Trifiro, J. Catal. 91 (1985) 85.
[12] G.I. Straguzzi, K.B. Bischoff, T.A. Koch and G.C.A. Schuit, J. Catal. 104 (1987) 47.
[13] I. Aso, S. Furukawa, N. Yamazoe and T. Seiyama, J. Catal. 64 (1980) 29.
[14] I. Aso, N. Yamazoe, T. Amamoto and T. Seiyama, in T. Seiyama and K. Tanabe (Eds.) Proceedings, 7th International Congress on Catalysis, Tokyo, 1980, Part B, Elsevier, Amsterdam/New York, 1981, p. 1239.
[15] N. Burriesci, F. Garbassi, M. Petrera and G. Petrini, J. Chem. Soc., Faraday Trans. 1, 78 (1982) 817.
[16] I. Aso, T. Amamoto, N. Yamazoe and T. Seiyama, Chem. Lett., (1980) 365.
[17] G.K. Boreskov, S.A. Vent'yaminov, V.A. Dzis'ko, D.V. Tarasova, V.M. Dindoin, M.M. Sazonova, T.P. Olen'kova and L.M. Kelefi, Kinet. Catal. 10 (1969) 1350.
[18] V.P. Shchukin, G.K. Boreskov, S.A. Ven'yaminov and D.V. Tarasova, Kinet. Catal. 11 (1970) 153.
[19] G. Centi and F. Trifiro, Catal. Rev.-Sci. Eng. 28 (1986) 165.
[20] M. Carbucicchio, G. Centi and F. Trifiro, J. Catal. 89 (1985) 107.
[21] Y.M. Cross and D.R. Pyke, J. Catal. 58 (1979) 61.
[22] G.M. Bartenev, R.R. Zakirov and A.D. Tsyganov, Sov. Phys. Solid State, 16 (1975) 2409.
[23] M. Hansen (Ed.), Constitution of Binary Alloys, McGraw-Hill, New York, 1958, p. 708.
[24] N.V. Ageev (Ed.), Hand Book of Binary Metallic Systems, Structure and Properties, Vol. II, 1967, p. 393. Translated from Russian by Isreal Programme for Scientific Translation, Jerusalem, 1967.
[25] T.B. Massalski (Ed.), Binary Alloys Phase Diagrams, Vol. II, American Society for Metals, Metals Park, OH 44073, 1986, p. 1104.
[26] I.A. Tumolillo, Phys. Status Solidi A, 17 (1973) 315.
[27] G.W. Keulks, J. Catal. 19 (1970) 232.
[28] W.C. Conner and C.O. Bennett, J. Catal. 41 (1976) 30.
[29] D.L. Doering, H. Poppa and J.T. Dickinson, J. Vac. Sci. Technol. 17 (1980) 198.
[30] D.L. Doering, J.T. Dickinson and H. Poppa, J. Catal. 73 (1982) 91.
[31] S. Ichikawa, H. Poppa and M. Boudart, J. Catal. 91 (1985) 1.
[32] E. Gillet, S. Channakhone and V. Matolin, J. Catal. 97 (1986) 437.
[33] I. Aso, M. Nakao, N. Yamazoe and T. Seiyama, J. Catal. 57 (1979) 287.
[34] I. Barin and I. Kanacke, Thermochemical Properties of Inorganic Substances, Springer Verlag, Berlin, 1973.
[35] R.C. Weast (Ed.), CRC Handbook of Chemistry and Physics, The Chemical Rubber Co., Cranwood Parkway, Cleveland, OH, 1968, F-158.
[36] L.-T. Weng, B. Zhou, B. Yasse, B. Doumain, P. Ruiz and B. Delmon, in M.J. Phillips and M. Ternan (Eds.), Proceedings, 9th International Congress on Catalysis, Calgary, 1988, Vol. 4, The Chemical Institute of Canada, Ottawa, 1988, p. 1609.
[37] M.M. Gadgil and S.K. Kulshreshtha, unpublished work.